Journal of Power Sources 196 (2011) 5546–5554

Contents lists available at ScienceDirect

Journal of Power Sources

journal homepage: www.elsevier.com/locate/jpowsour

Gadolinia-doped ceria mixed with alkali carbonates for solid oxide fuel cell applications: I. A thermal, structural and morphological insight

M. Benamira[a], A. Ringuedé[a], V. Albin[a], R.-N. Vannier[c], L. Hildebrandt[b], C. Lagergren[b], M. Cassir[a,*]

[a] Laboratoire d'Electrochimie, Chimie des Interfaces et Modélisation pour l'Energie, UMR 7575 CNRS, Chimie ParisTech, 11 rue Pierre et Marie Curie, F-75231 Paris Cedex 05, France
[b] KTH Chemical Science and Engineering, Department of Chemical Engineering and Technology, SE-100 44 Stockholm, Sweden
[c] Unité de Catalyse et de Chimie du Solide, UMR 8181 CNRS, Villeneuve d'Ascq, France

ARTICLE INFO

Article history:
Received 3 September 2010
Received in revised form 18 January 2011
Accepted 2 February 2011
Available online 22 February 2011

Keywords:
SOFC
Composite
Alkali molten carbonates
Gadolinia-doped ceria
Structural and thermal analyses

ABSTRACT

Ceria-based composites are developed and considered as potential electrolytes for intermediate solid oxide fuel cell applications (ITSOFC). After giving a survey of the most relevant results in the literature, the structural, thermal and morphological properties of composite materials based on gadolinia-doped ceria (GDC) and alkali carbonates (Li_2CO_3–K_2CO_3 or Li_2CO_3–Na_2CO_3) are carefully examined. Thermal analyses demonstrate the stability of the composite with very low weight losses of both water and CO_2 during thermal cycling and after 168 h ageing. High-temperature and room-temperature X-ray diffraction allowed determining the precise structure of the composite and its regular and reversible evolution with the temperature. The microstructure and morphology of electrolyte pellets, as observed by scanning electron microscopy (SEM), show two-well separated phases: nanocrystals of GDC and a well-distributed carbonate phase. Finally, electrical conductivity determined by impedance spectroscopy is presented as a function of time to highlight the stability of such composites over 1500 h.

1. Introduction

Development of intermediate-temperature solid oxide fuel cells (ITSOFC), operating at $T < 700\,^{\circ}C$ requires a new generation of electrolytes. Ceria-based electrolytes, such as gadolinia-doped ceria (GDC) or samaria-doped ceria (SDC) are among the most interesting oxide-conducting electrolytes at these temperatures. Their ionic conductivity of about 10^{-2}–$2 \times 10^{-2}\,S\,cm^{-1}$ at 600 °C is higher than that of the conventional material used for high temperature SOFC electrolyte, YSZ (yttria stabilized zirconia, about $5 \times 10^{-3}\,S\,cm^{-1}$ at the same temperature) [1]. Nevertheless, their ionic conductivity is still ten times lower than the goal value of $10^{-1}\,S\,cm^{-1}$. Moreover, ceria-based electrolytes, due to the reduction of Ce^{4+} into Ce^{3+} under the SOFC anode reducing atmosphere, are also electronic conductors, which limit their use. In the last decade, promising composite materials based on mixtures of stabilized zirconia or ceria and alkali carbonate salts were developed and analysed for their use as electrolyte materials in SOFCs. In particular, GDC or SDC were mixed with chlorides [2–6], fluorides [2,3], carbonates [3–33] and sulphates [34]. According to the literature, these composite materials, with enhanced ionic conductivity, are supposed to conduct both oxygen ion and protons. The carbonate eutectic being molten or partially molten at intermediate temperature (>500 °C) would create an interfacial conduction pathway. Oxide ions ensure the conductivity in the oxide phase; meanwhile the conductivity is attributed to protons in the carbonate phase. In fact, no rigorous explanation has been given yet on the transport conduction mechanisms [2–14]. It should nevertheless be outlined that many interesting studies have been published in the very recent years and an overview will be given before introducing our main objectives. Li and Sn have developed a so-called NANOSOFC, based on a composite with nano-SDC salt mixed with a Li–Na carbonate eutectic [16]. A maximum output power density of $140\,mW\,cm^{-2}$, stable for 200 h, was reached at 650 °C. Different groups co-authored with Zhu have analysed thoroughly the influence of particle size, synthesis procedure and morphology on the performance and stability of SDC-based composite cells [17–21]. For instance, Tang et al. observed that composites with particles size at nano-scale level showed enhanced conductivities at low temperatures but more complex boundaries effects with respect to particles of the micrometer level [17]. Lapa et al. synthesised and characterised nano-composites also based on SDC and Li–Na carbonates [18]. These mixtures showed impressive levels of conductivity and a complex distribution of the two phases: a ceramic skeleton of bonded nano-sized grains surrounded by the carbonate phase. Di et al. studying the conductivity, morphology and cell performance of the same kind of composites, observed a sharp increase in the conductivity related to a superionic phase transition in the interface between SDC and carbonates phases [19]. The cell reached a maximum power density of $590\,mW\,cm^{-2}$ at 600 °C. Raza et al. showed

* Corresponding author. Tel.: +33 1 55426387; fax: +33 1 44276750.
E-mail address: michel-cassir@chimie-paristech.fr (M. Cassir).

0378-7753/$ – see front matter © 2011 Elsevier B.V. All rights reserved.
doi:10.1016/j.jpowsour.2011.02.004

that the use of Na_2CO_3 as the carbonate phase improved significantly the performance with respect to Li–Na carbonate eutectic, reaching 1.15 W cm^{-2} at 500 °C [20]. Ma et al. analysed the thermal stability of SDC/Na_2CO_3 nanocomposites, showing that Na_2CO_3 phase exists steadily in the SDC phase: a stable power density of 0.62 W cm^{-2} was obtained over 12 h [21]. Huang et al. analysed different features of the behaviour of SDC/Li–Na composites [22–26]. In a first study, the authors tested an anode-supported cell (NiO) with an SDC/Li–Na composite electrolyte and a $Li_xNi_{1-x}O$ cathode; they obtained an open-circuit voltage (OCV) of 1.04 V and a steady output of 0.5 W cm^{-2} at 550 °C for about 35 h [22]. In a similar study, Huang et al. also showed that the performance of such cells increased with the carbonate content in the composite electrolyte, e.g. a performance of 1.085 W cm^{-2} was reached at 600 °C with 25 wt% of carbonates [23]. The authors claimed that during the fuel cell operation, the electrolyte is a co-ionic (O^{2-}/H^+) conductor. Huang et al. analysing again the same kind of cell but with an excess of Li_2CO_3 with respect to Na_2CO_3, found that an increase in the electrolyte thickness is favourable to cell performance (higher OCV and power density) [24]. In the range of 400–600 °C, for this composite material, the proton conduction was found to be predominant and assumed to occur through the cationic vacancy in the interfacial regions of the electrolyte. Furthermore, Huang et al. studied the effect of the carbonate composition on the electrical properties of the composite electrolytes [25]. The performance of cells including these electrolytes showed that the best carbonate mixture is Li–Na (600 mW cm^{-2} at 600 °C), followed by Li–K and Na–K. Huang et al. also showed that lanthanum nickelates doped with cobalt are well-adapted cathodes for SDC/Li–Na (67–33 mol%) composite electrolytes [26]. The research group of Li also was interested by the use of SDC/carbonates composites for SOFC devices, as direct carbon fuel cell and as CO_2 permeation membrane [27–30]. The high power output obtained with a cell including SDC/Li–Na composite, 1.7 W cm^{-2} at 650 °C with 3 A cm^{-2} [27], has to be outlined. Also interesting performances were obtained with SDC/Li–Na–K composite (1.7 W cm^{-2} at 650 °C) with evidence, according to the authors, for a ternary ionic conduction due to O^{2-}, CO_3^{2-} and H^+ [28]. The influence of the composite morphology according to the preparation technique on the thermal and ionic transport was described, showing also the interest of using thin layered-composites [29]. The same group also employed the same composite as electrolyte in direct carbon fuel cell, obtaining a power output of 100 mW cm^{-2} at 700 °C [30]. Zhang analysed the behaviour of a co-doped ceria $Ce_{0.8}Gd_{0.05}Y_{0.15}O_{1.9}$ mixed with Li–Na carbonate, obtaining a power density of 670 mW cm^{-2} at 550 °C [31]. The durability of a cell with the same composite material was also tested during 135 h, with a maximum power density decreasing from 520 to 300 mW cm^{-2} at 550 °C [32]. Liu, analysing the behaviour of another co-doped ceria, $Ce_{0.8}Sm_{0.1}Nd_{0.1}O_{1.9}$, mixed with Li–Na carbonates explained that the conductivity enhancement is due to the increase in the number of oxygen transfer routes at the interface between doped-ceria and carbonates [33].

Although interesting results have been obtained in varied topics concerning the composite, it is still difficult to fully understand the behaviour of such a mixed electrolyte. What is the real mechanism and how does it work? Why do some authors mention a proton conduction within the carbonate phase? Furthermore, the mentioned performances are quite dispersed and also the values of conductivity rarely compared rigorously to the literature. In this work, the aim of our groups, specialized in electrochemistry and high-temperature fuel cells, SOFC and MCFC, was to thoroughly analyse the chemical/electrochemical properties of varied compositions of the mixtures GDC/Li_2CO_3–K_2CO_3 and GDC/Li_2CO_3–Na_2CO_3, with different experimental conditions (synthesis of the melt, gas atmosphere, temperature, etc.). This was done in order to have a deeper insight on the behaviour of these composites and as an attempt elucidating the ionic transport phenomena responsible of the enhanced conductivity. This study will be developed through a serial of two papers. A careful examination of the structural, morphological and thermal behaviour of the composites will be described in this first paper, as well as the ageing behaviour (conductivity vs. time) in a range of 1500 h, longer than in all the cited papers. The second one will be dedicated to a thorough electrochemical study by impedance spectroscopy in order to analyse in different conditions (oxidant and reductive atmospheres, annealing temperature, cycling, ageing.) the electrical and electrochemical characteristics of such new electrolytes.

2. Selection of the alkali carbonates mixtures

A basic knowledge on alkali carbonates media is essential for a better understanding of the composite properties. Single alkali carbonates are Li_2CO_3, Na_2CO_3 and K_2CO_3, with melting points of 730, 901 and 858 °C, respectively [34]. Their eutectic mixtures, mainly Li_2CO_3–K_2CO_3 and Li_2CO_3–Na_2CO_3, are used as molten carbonate fuel cell electrolyte. The phase diagrams of such melts show two eutectic compositions for Li_2CO_3–K_2CO_3 (62–38 mol% or 42.8–57.2 mol%) and only one for Li_2CO_3–Na_2CO_3 (52–48 mol%) [34]. The melting points of Li–K eutectics are 488 and 499 °C, respectively, and that of the Li–Na eutectic, 501 °C [34,35]. It has also been shown by Nastase et al. that the conductivity of the molten carbonate greatly depends on the nature of the alkali cation, e.g. $\sigma_{Li_2CO_3} > \sigma_{Na_2CO_3} > \sigma_{K_2CO_3}$, respectively 5.4, 2.8 and 2 S cm^{-1} at 900 °C [36]. The same authors showed that Li_2CO_3–Na_2CO_3 is a better conductor than Li_2CO_3–K_2CO_3 and that the conductivity of the latter increases with the amount of Li_2CO_3. Consequently, conductivity-related activation energy of Li_2CO_3–K_2CO_3 (80–20 mol%) is significantly lower than that of Li_2CO_3–K_2CO_3 (62–38 mol%), 0.16 and 0.26 eV, respectively at 900 °C [36]. Based on these properties, we have selected two carbonate melts to be mixed with the GDC phase. The first one is Li_2CO_3–K_2CO_3 (72.7–27.3 mol%), with an excess of lithium carbonate with respect to the 62–38 mol% eutectic composition. In a temperature range of 500–600 °C, this mixture is composed by the molten eutectic containing an excess of Li_2CO_3 in a solid-state, as revealed by XRD diagrams, not shown in this paper. By selecting this composition, we hoped to obtain a better mechanical behaviour of the resulting pellets as well as a better chemical stability of the different GDC–carbonates composite phases with respect to the eutectic composition. Finally, after numerous assays, the behaviour of this composition was compared to that of the eutectic without finding any significant change neither with respect to the mechanical strength nor the performance. Therefore, the GDC mixed with Li_2CO_3–K_2CO_3 (72.7–27.3 mol%) composite with an excess of lithium will be presented here. The second composite was GDC mixed with the Li_2CO_3–Na_2CO_3 (52–48 mol%) eutectic. The two composites should allow comparing the effect of the carbonate nature and composition on the composite properties.

3. Experimental

3.1. Preparation of GDC–carbonate composite electrolyte

The composite electrolytes were prepared by a solid-state reaction. Li_2CO_3, K_2CO_3 and Na_2CO_3, Sigma–Aldrich reagents of high purity (≥99.8%), were used. The first composition of carbonates was prepared by mixing Li_2CO_3 and K_2CO_3, at a molar ratio of 72.7/27.3, and heating it at 650 °C/60 min in air/CO_2 (30/70). Then, the as-prepared carbonate salt and a powder of gadolinium-doped ceria

($Ce_{0.9}Gd_{0.1}O_{1.9}$, GDC) (Rhodia, France), of high purity (99.9%), were mixed together in different weight ratios: 80/20, 70/30 and 60/40 GDC/composite. The mixture was ground in a mortar and heated at 650 °C in air/CO_2 for 40 min, with a heating rate of 2 °C min^{-1}. The resulting samples were taken directly from the furnace to room temperature and ground again thoroughly to be used as electrolyte. In order to analyse the influence of heat treatment temperature on the microstructure, mixtures were also annealed at 600 and 680 °C in air/CO_2 for 40 min or at 650 °C for 60 min. The second carbonate mixture was Li_2CO_3–Na_2CO_3 (52–48 mol%) with a molar fraction corresponding to the eutectic. The preparation technique was the same as for GDC/Li_2CO_3–K_2CO_3.

All the annealed powders were pressed into pellets at a uniaxial pressure of 30 MPa. The pellets were then sintered at 600 °C for 1 h in air, with a heating and a cooling rate of 5 °C min^{-1}.

3.2. Structural morphological and characterisations of the composite electrolytes

Room-temperature and high-temperature X-ray diffraction (HT-XRD) were used to characterise the composite samples.

The X-ray diffraction (XRD) patterns of the composite electrolytes were recorded at room temperature using a Philips PW 1390 diffractometer using the Co K_α radiation (λ = 1.78897Å) with 2θ varying from 25 to 65°, with a step of 0.02° and 3 s counting time per step.

The HT-XRD patterns of the composite electrolytes were collected using a D8 Bruker diffractometer equipped with an Anton Paar HTK1200 N furnace and a Vantec1 linear detector, with the Cu K_α radiation (λ = 1.54056 Å) and 2θ varying from 20 to 75° by steps of 0.0146°. Each pattern was collected in 15 min. Measurements were carried out between 25 and 650 °C each 25 °C, under air flow (5 L h^{-1}) on heating and cooling with a rate of 0.1 °C s^{-1} between each temperature step. To avoid any reaction with the alumina sample holder, the sample was deposited on a gold sheet.

Scanning electron microscopy, SEM (S440, FEG from LEICA), coupled with energy-dispersive X-ray spectrometry, EDS (S440, FEG from LEICA) was used to investigate the morphology of the different samples.

3.3. Thermal analyses of carbonates and composite electrolytes

Thermo-gravimetric analysis–differential thermal analysis (TGA–DTA) coupled with mass spectrometry were carried out on a TGA–DTA (Thermo gravimetric analysis–Differential thermal analysis) Setaram 92 thermal analyzer at a rate of 5 °C min^{-1}–700 °C on heating and cooling. Platinum crucibles were used. When mass spectrometry (Omnistar, Pfeiffer) was employed to characterise the exhaust gas, experiments were carried out under argon; in other case, air was used. No difference was observed when the atmosphere was changed.

3.4. Electrical performance

Electrical measurements were performed by electrochemical impedance spectroscopy (EIS). The measurements were realized using a Solartron 1287 potentiostat. The signal amplitude was fixed at 20 mV in respect to the system linearity, in the 50 kHz–0.5 Hz frequency range, with 11 points per decade. Measurements were carried out as a function of temperature; under ambient atmospheric air. Arrhenius plots of the conductivity and evolution of conductivity vs. time were presented.

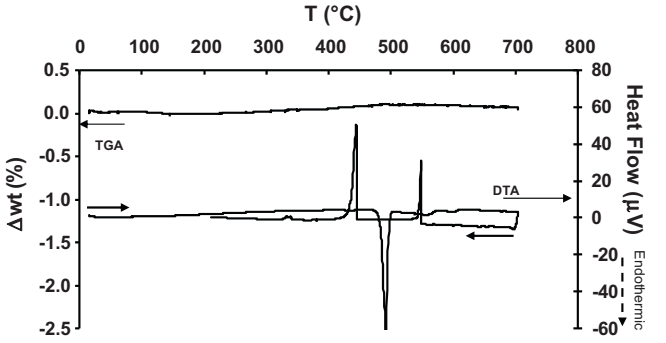

Fig. 1. TGA and DTA plots of the carbonate mixture Li_2CO_3–K_2CO_3 (72.7/27.3), annealed at 650 °C for 60 min. The experiment was carried out under argon with a rate of 5 °C min^{-1}.

4. Results and discussion

4.1. TGA and DTA analyses

4.1.1. GDC with Li_2CO_3–K_2CO_3 (72.7/27.3) mol% composite

In a first step, DTA and TGA analyses coupled to mass spectrometry were performed on the mixture of carbonate powders in order to determine their physical and chemical transformations during thermal cycling and to check their stability in such conditions.

Fig. 1 depicts the thermal analysis behaviour of Li_2CO_3–K_2CO_3 (72.7/27.3 mol%). The DTA plot shows an intense peak at 485 °C, corresponding to the melting point of the Li_2CO_3–K_2CO_3 (62–38 mol%) eutectic, in good agreement with the literature (488 °C). Afterwards, a more dispersed signal, corresponding to the progressive melting of Li_2CO_3 (in excess with respect to the eutectic composition) up to 590 °C, can be observed. During the cooling process, the two exothermic peaks at 547 °C and 440 °C can be attributed to the beginning of Li_2CO_3 crystallisation and to the end of the eutectic formation. In the TGA plot, the low signal corresponding to the weight loss, lower than 0.1%, shows evidence of the good stability of the carbonate mixture. However, as seen in Fig. 2 from mass spectrometry, an increase in the signal corresponding to mass 44 (CO_2) is to be noticed beyond 490 °C and is associated to a progressive loss of CO_2, of about 0.03%. At 140 °C, small signals are also to be noticed for mass 18 (H_2O) and 44 (CO_2). It is difficult to quantify the amounts of water and carbon dioxide by mass spectrometry, the scales of the given signals being different from a compound to another. However, the height of the signal observed at 140 °C for mass 44 can be compared to that of the signal observed beyond 490 °C; it is 10 times lower and one may conclude that, at this tempera-

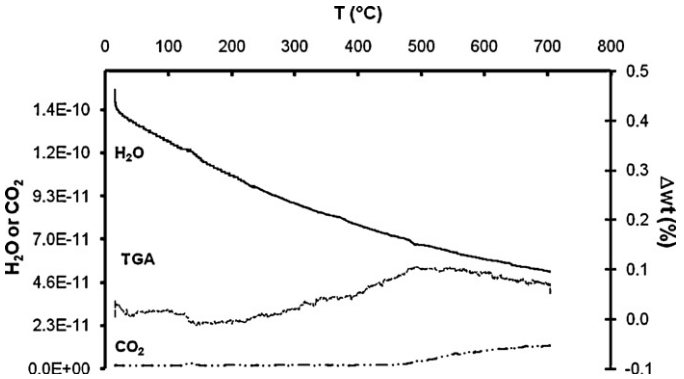

Fig. 2. TGA and mass spectra of the carbonate mixture Li_2CO_3–K_2CO_3 (72.7/27.3), annealed at 650 °C for 60 min. The experiment was carried out under argon with a rate of 5 °C min^{-1}.

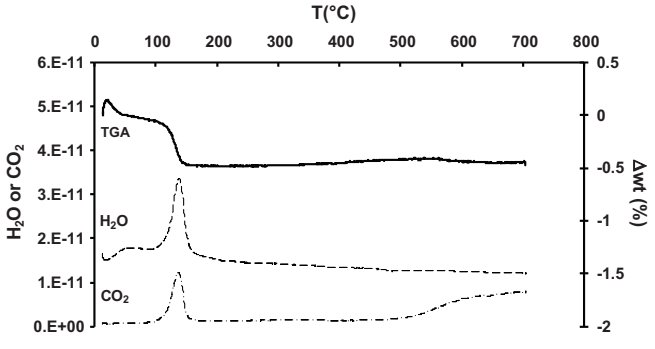

Fig. 3. TGA and mass spectra of the GDC/Li_2CO_3–K_2CO_3 (80/20 wt%) composite, annealed at 650 °C for 60 min. The experiment was carried out under argon with a rate of 5 °C min^{-1}.

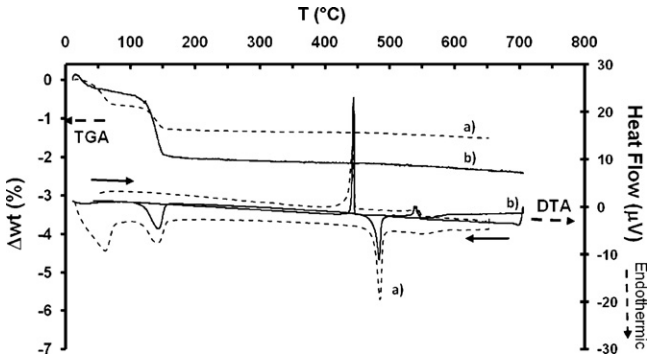

Fig. 5. TGA and DTA plots of the GDC/Li_2CO_3–K_2CO_3 composite, with two compositions: (a) 70/30 wt% and (b) 80/20 wt%. Annealing at 650 °C for 60 min. The experiment was carried out under air with a rate of 5 °C min^{-1}.

ture, it is mainly water which is released, with some traces of CO_2.

Fig. 3 shows the TGA and mass spectrometry analyses of the GDC/Li_2CO_3–K_2CO_3 (80/20 wt%) composite. In this case, the weight loss at 140 °C, of around 0.4%, becomes more important and corresponds to the release of both H_2O and CO_2. The ratio between H_2O and CO_2 signals is 1.2. As for the carbonate alone, an increase in the signal corresponding to mass 44 (CO_2) is also noticed beyond 500 °C. One may estimate the amount of CO_2 released at 140 °C, by comparing the height of the signal of molar mass 44 (CO_2) at this temperature with that observed beyond 500 °C, which is about 0.05%. It can be concluded that the weight loss at 140 °C is also mostly due to water, as for Li_2CO_3–K_2CO_3 alone.

In Fig. 4, DTA and TGA analyses of the composite carried out under argon are compared to those of the carbonate mixture. The weight loss is more important in the case of the composite, which can be explained by the release of water adsorbed on the surface of the GDC powder. The peaks observed at high temperature are close to those of the carbonate melt, which allows ascribing them to the carbonate phase and to the different phase changes occurring during the heating/cooling cycle of the Li_2CO_3–K_2CO_3 mixture. Knowing that the composite analysed contains only 20 wt% of carbonates, the weakness of the peak signals with respect to the carbonate phase can be easily understood.

TGA and DTA analyses of the 80/20 wt% composite samples annealed at 600 or 680 °C for a duration of 40 min, were also carried out, but are not shown here. All the plots are similar, showing a weight loss at 140 °C related to the dehydration of ceria and endothermic peaks characteristic of the melting point of the Li_2CO_3–K_2CO_3 (62–38 mol%) eutectic. However, the water release varied according to the heat treatment, being more important for the sample annealed at 650 °C. This difference of behaviour is likely due to different moisture of GDC in the composites and is probably not related to the temperature of annealing.

In Fig. 5, two compositions of the GDC/Li_2CO_3–K_2CO_3 composite were analysed by TGA and DTA under air: 70/30 wt% and 80/20 wt%. The weight loss at 140 °C, around 2%, is more accentuated for the composition containing 20 wt% of carbonates, which confirms the assignation of this loss to the release of water from the GDC phase. No shift in the temperature of the transitions associated to the carbonates mixture is observed and the intensities of these peaks are in good agreement with the composites composition.

Fig. 6 shows the TGA and DTA analyses of the GDC/Li_2CO_3–K_2CO_3 (80/20 wt%) composite after ageing during 168 h at 500 °C under air. The shape of the curves is almost the same than before ageing (Fig. 5b) with, in particular, a low weight loss (about 0.3%) at 140 °C and an intense endothermic peak at 485 °C corresponding to the melting point of the Li_2CO_3–K_2CO_3 (62–38 mol%) eutectic. These observations prove the presence of carbonates and the stability of the composite after this ageing treatment.

4.1.2. GDC with Li_2CO_3–Na_2CO_3 (52–48 mol%) composite

In Fig. 7, DTA and TGA analyses of the GDC/Li_2CO_3–Na_2CO_3 composite are compared to those of the pure carbonate eutectic. The weight loss of 2% found for the composite can be attributed to the release of adsorbed water from the surface of the GDC powder as for the other composites. The melting point of the pure carbonate melt (500 °C) is in good agreement with the literature [34,35]. A slightly lower value is obtained for the composite, as shown in Fig. 7.

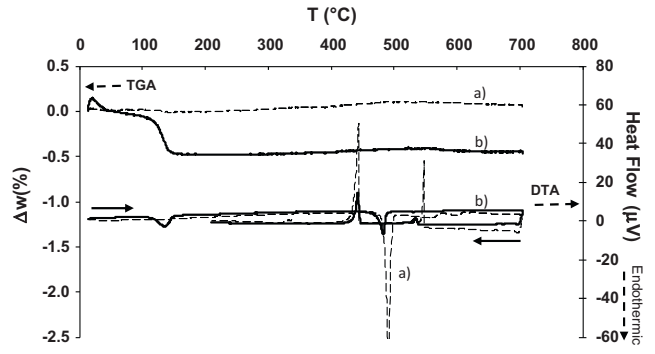

Fig. 4. TGA and DTA plots of the carbonate mixture Li_2CO_3–K_2CO_3 (72.7/27.3 mol%) (a) compared to the GDC/Li_2CO_3–K_2CO_3 (80/20 wt%) composite (b). Annealing at 650 °C for 60 min. The experiment was carried out under argon with a rate of 5 °C min^{-1}.

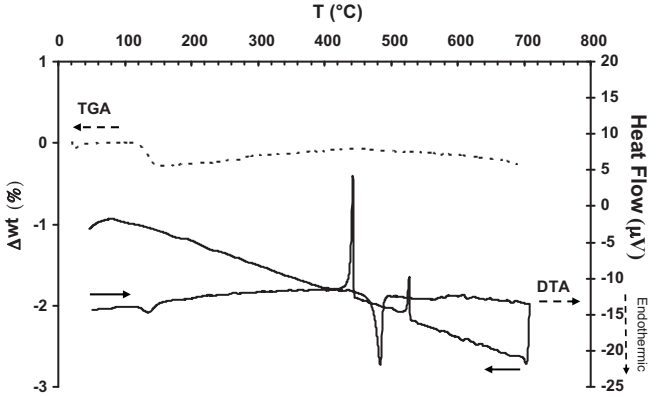

Fig. 6. TGA and DTA plots of the GDC/Li_2CO_3–K_2CO_3 (80/20 wt%) composite after ageing at 500 °C during 168 h. Annealing at 650 °C for 60 min. The experiment was carried out under argon with a rate of 5 °C min^{-1}.

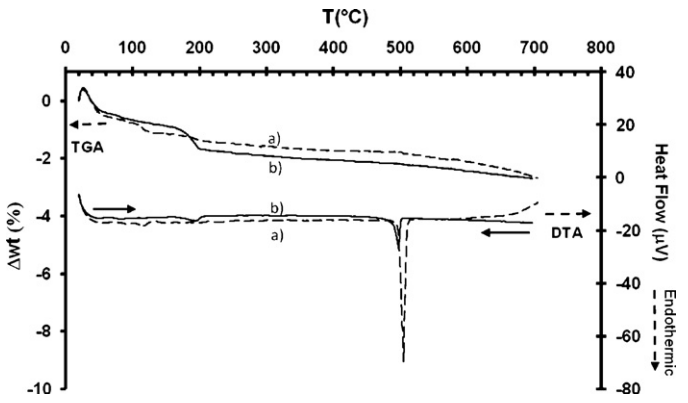

Fig. 7. TGA and DTA plots of the carbonate mixture Li_2CO_3–Na_2CO_3 (52–48 mol%) (a) compared to the GDC/Li_2CO_3–Na_2CO_3 (80/20 wt%) composite (b). Annealing at 650 °C for 60 min. The experiment was carried out under air with a rate of 5 °C min^{-1}.

4.2. XRD analyses

To complete this thermal analysis, High-temperature XRD was also carried out up to 650 °C under air. Because of the low scattering of the carbonates compared to ceria, only the results corresponding to the GDC/Li_2CO_3–K_2CO_3 70/30 wt% composition are discussed here. Fig. 8 reports the XRD patterns of a composite: GDC/Li_2CO_3–K_2CO_3 (70/30 wt%) annealed at 650 °C for 1 h. At room temperature, small peaks in the background of the GDC patterns were identified as Li_2CO_3 (PDF: 00-022-1141) and $(Li_{0.5}K_{0.5})_2CO_3$ (PDF: 01-087-0731), in good agreement with the expected carbonate melt composition (Fig. 8a). In order to better identify Li_2CO_3 Bragg peaks at high temperature, a high temperature X-ray diffraction study was carried out on Li_2CO_3 alone in the same conditions as for the mixture with GDC from room temperature to 500 °C. Corresponding diagrams are given in Fig. 8b. On heating, the peaks corresponding to the carbonates disappear above 525 °C and only traces of Li_2CO_3 (PDF: 00-022-1141) are still present between 475 and 525 °C. Although a small shift in temperature, XRD were collected every 25 °C only, these two transitions are in good agreement with the temperatures observed by thermal analyses for the melting of the eutectic and the progressive melting of Li_2CO_3. On cooling, the reverse process is confirmed with the appearance of Li_2CO_3 peaks below 525 °C (in good agreement with the exothermic peak observed at 547 °C by DTA) and the crystallisation of a new phase at 425 °C (in good agreement with the second exothermic peak observed by DTA at 440 °C). It was not possible to identify the phase formed below 425 °C with the X-ray database. A further transition was noticed around 200 °C that could not be identified either. It is also worth noting that an increase in the height of the GDC Bragg peaks associated to a decrease in their full width at half maximum was observed above 575 °C, indicating an increase in the crystallite size of the GDC phase (Fig. 8c). The first collected pattern

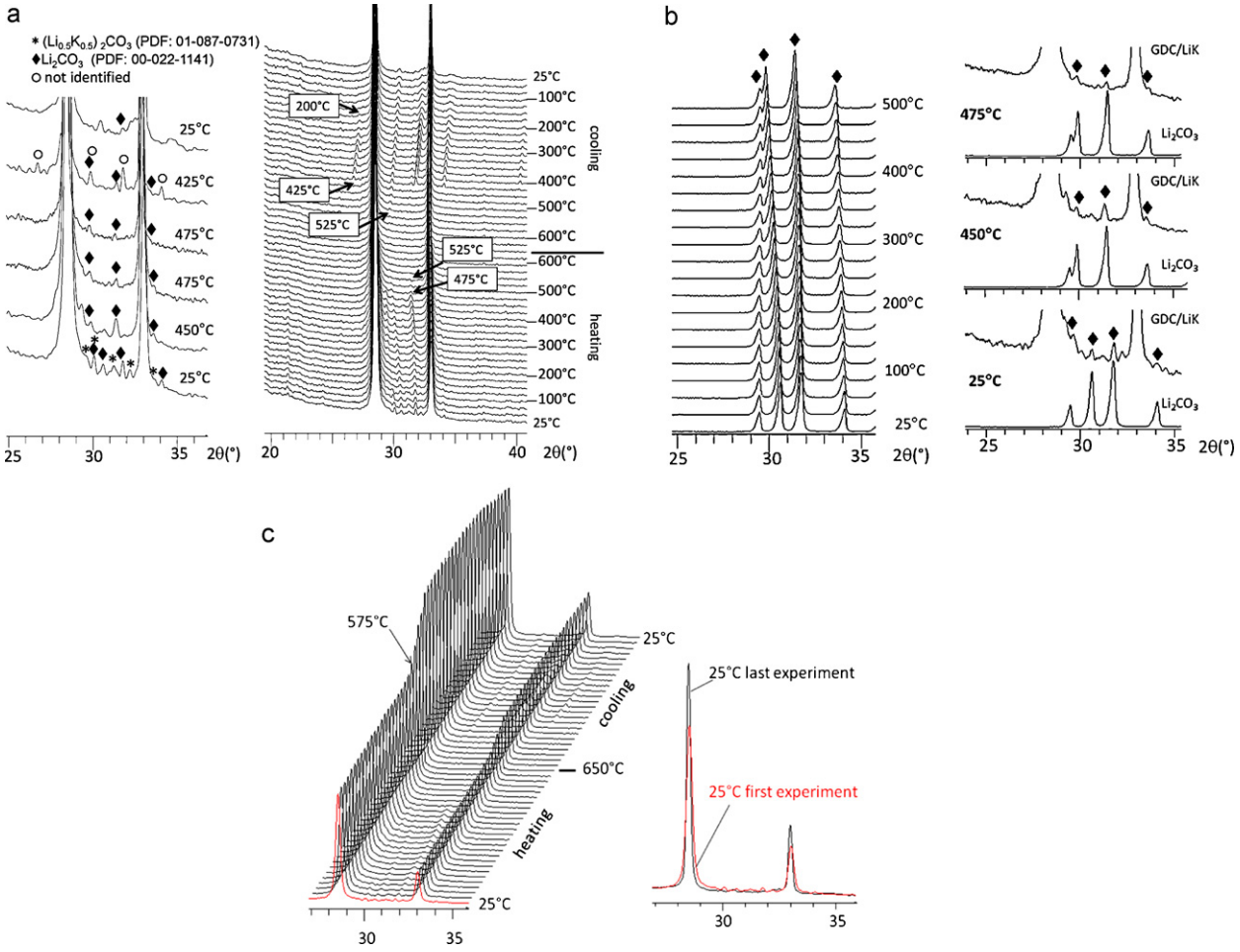

Fig. 8. XRD patterns as a function of temperature relative to a GDC/Li_2CO_3–K_2CO_3 (70/30 wt%) composite (annealed at 650 °C for 60 min). (a) 2D plot showing the main peaks corresponding to carbonates, (b) Li_2CO_3 XRD patterns as a function of temperature collected in the same conditions as the composite from RT to 500 °C and comparison with the composite at selected temperatures and (c) 3D plot showing the evolution of the intensity of GDC Bragg peaks with a comparison between the XRD patterns at 25 °C before heating (red) and after cooling (black). (For interpretation of the references to colour in this figure legend, the reader is referred to the web version of this article.)

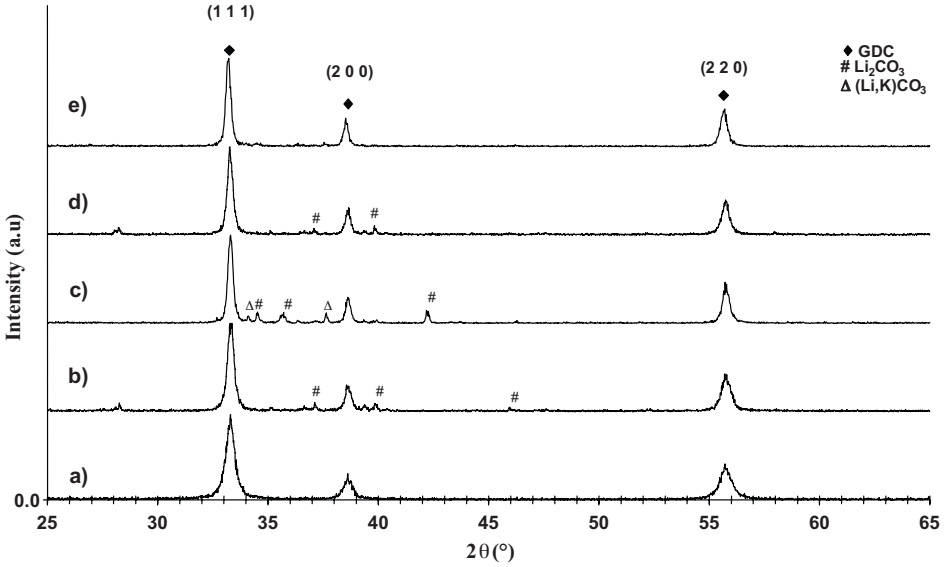

Fig. 9. XRD patterns of (a) pure GDC powder; (b) GDC–composite annealed at 650 °C for 40 min, before sintering; (c) same sample after sintering at 600 °C for 60 min; (d) GDC–composite annealed at 680 °C for 40 min; (e) same sample after sintering at 600 °C for 60 min.

and the last collected pattern are compared in Fig. 8c. The small shift observed for the GDC Bragg peak positions can be explained by a height shift of the sample due to the carbonate melting. The study of the average size strain plots corresponding to these two patterns based on the Halder–Wagner–Lanford model [37] confirmed an increase in the crystallite size of GDC from 26 nm before the high temperature study to 48 nm after the experiment. Interestingly, microstrain was also observed, it decreases from 0.7% before to 1% after experiment. Despite some small changes in the Bragg peaks intensity, likely due to different preferred orientations of the carbonate phases, the same phase transitions for the carbonates and the same evolution of the GDC Bragg were observed for other composites, GDC/Li_2CO_3–K_2CO_3 (70/30 wt%) annealed at 650 °C or 680 °C for different times, confirming the melting of the carbonates above 550 °C and the reversibility of the transformation.

Fig. 9 shows the XRD patterns of a pure GDC powder, GDC/Li_2CO_3–K_2CO_3 (80/20 wt%) composite electrolytes (GDC–composite) annealed at 650 °C or 680 °C for 40 min and the corresponding pellets sintered at 600 °C for 1 h. Thinner Bragg peaks after annealing are confirmed for all samples. The small peaks appearing in most of the XRD patterns are attributed to carbonates, either in a Li_2CO_3 or in a Li_2CO_3–K_2CO_3 form but intensities differ as shown during the high temperature study likely due to some different preferred orientation for the carbonates. In the case of the sample annealed at 650 °C during 40 min, b and c in Fig. 9, the carbonate peaks appear clearly after the sintering process at 600 °C. This indicates a better crystallinity of the carbonates after post-annealing. For samples annealed at higher temperature, 680 °C, as shown in Fig. 9, curve d, the carbonate peaks are less visible, even after a post-annealing at 600 °C, which could be due to a partial evaporation of the carbonates at the surface of the sample or to a more amorphous structure.

4.3. SEM analyses of the composite pellets

SEM analyses (with back-scattered electrons) of a GDC/Li_2CO_3–K_2CO_3 (80/20 wt%) composite pellet, heat-treated at 650 °C during 40 min, are depicted in Fig. 10. These micrographs show that both carbonate and oxide phases are well-separated and present different grain sizes. The localisation of both phases was determined by the contrast method. The heaviest atoms (cerium and gadolinium) re-emit more electrons than the lightest (those of carbonates, except lithium which is too light to be observed). Therefore, the zones corresponding to the heaviest atoms, GDC, are brighter. The darker areas, which can be fully isolated or in-between the GDC crystals, correspond to the carbonate phase. Before sintering the composite samples, see Fig. 9a and b, the white phase is constituted by small grains of GDC; whereas, the areas relative to the carbonate phase are divided in (i) an agglomerate distribution corresponding to the molten phase and (ii) dark grains, distributed among the GDC particles, corresponding to non-molten carbonates. After sintering the composite pellet at 600 °C for 1 h in air, SEM micrographs (Fig. 9c and d) show well-separated sub-micrometric particles of gadolinium-doped ceria and a well-distributed and uniform lithium/potassium carbonate mixture. The sintered material becomes denser and the separation of both phases more evident.

In the case of sintered GDC/Li_2CO_3–Na_2CO_3 (80/20 wt%), the magnification of zones 1 and 2 in Fig. 11 shows the regular distribution of the molten carbonate phase within the GDC phase. Both phases are even easier to identify than in the previously analysed composite.

4.4. Electrical performance and stability

Typical Nyquist impedance diagrams corresponding to GDC/Li_2CO_3–K_2CO_3 composite 80/20 wt% (annealed at 650 °C for 40 min) are shown in Fig. 12a at 390 °C and for different amplitudes. As can be observed, all the impedance curves at high frequencies are the same due to the lack of influence of the signal amplitude variation. This response is attributed to the contribution of the electrolyte and allows measuring its resistance and conductivity. At low frequencies, the impedance curves evolve with the amplitude applied and, consequently, the phenomenon can be ascribed to the polarization process at the electrode. At higher temperature above the carbonate mixture melting point, the impedance spectra have a different shape (not shown here). The first semi-circle, in the high frequency range, becomes very small and difficult to describe; whereas, the second one is predominant at medium and low frequencies. In this case the resistance corresponding to the electrolyte is measured at the first intercept between the Nyquist diagram and the Z′ real axis.

The conductivity of the GDC/Li_2CO_3–K_2CO_3 composite with three compositions: 80/20, 70/30 and 60/40 wt%, annealed at 650 °C

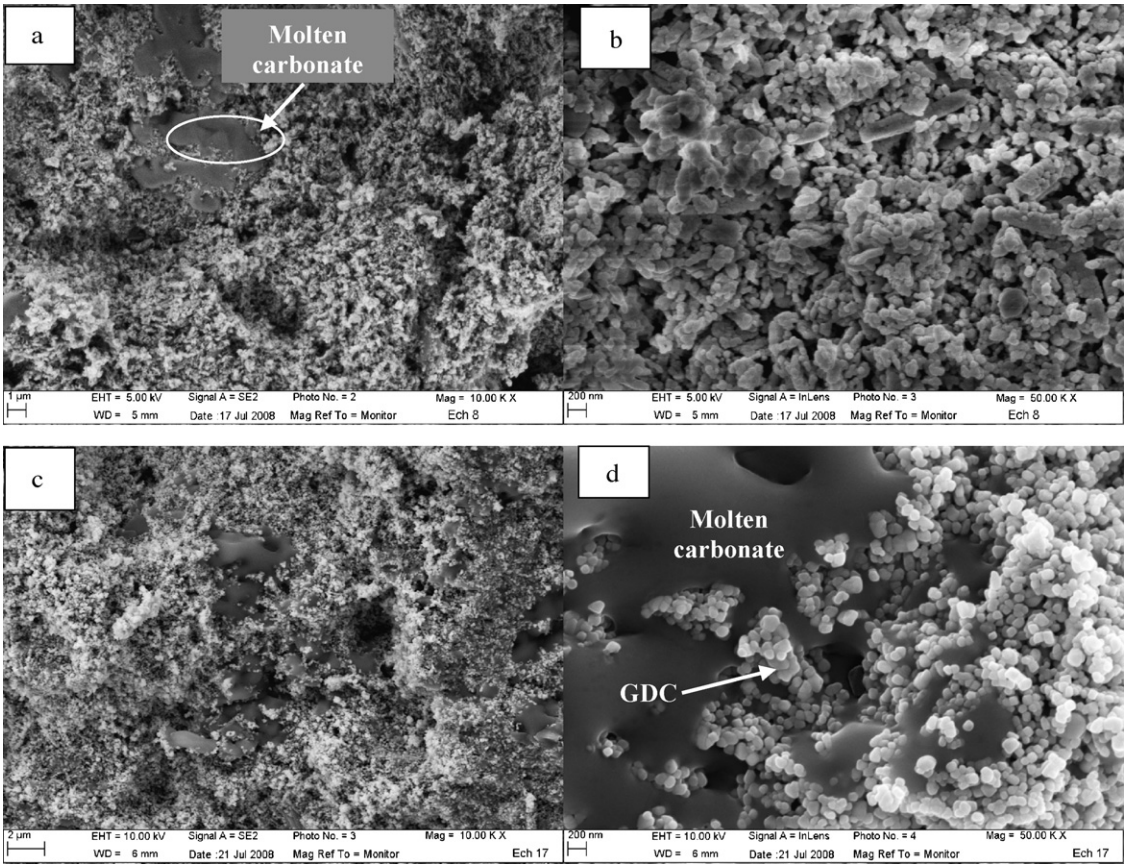

Fig. 10. SEM micrographs of the cross-section of the fractured surface of GDC/Li_2CO_3–K_2CO_3 (80/20 wt%) composite (a) and (b) before sintering; (c) and (d) after annealing.

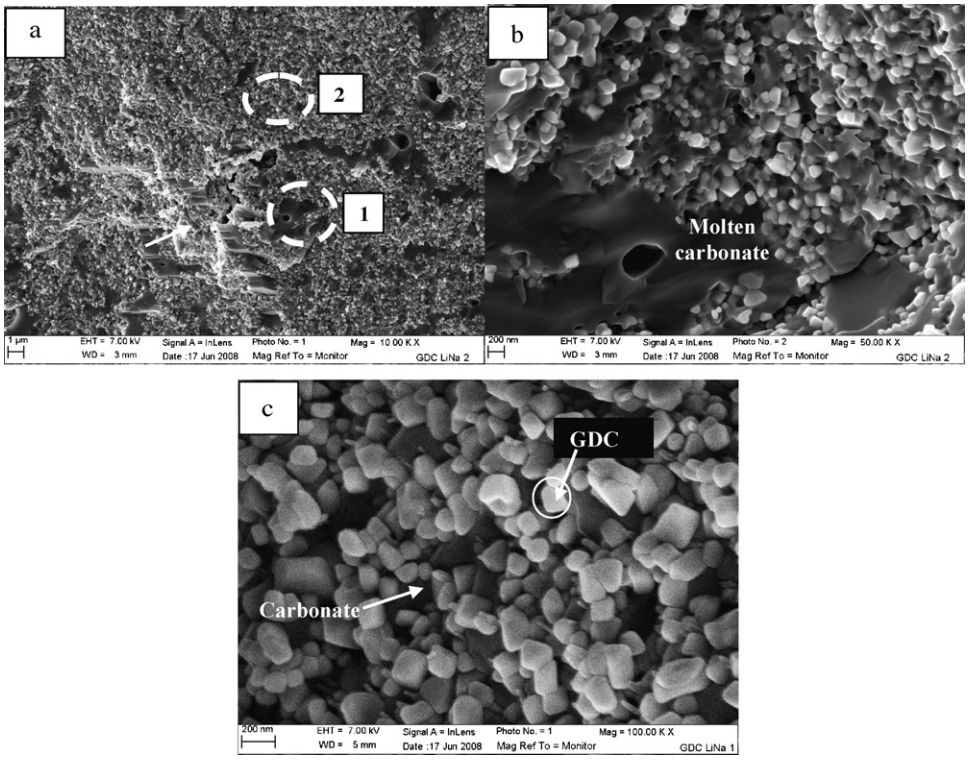

Fig. 11. SEM micrographs of the cross-section of the fractured surface of GDC/Li_2CO_3–Na_2CO_3 (80/20 wt%) composite after sintering: (a) general view; (b) enlargement of detail 1; (c) enlargement of detail 2.

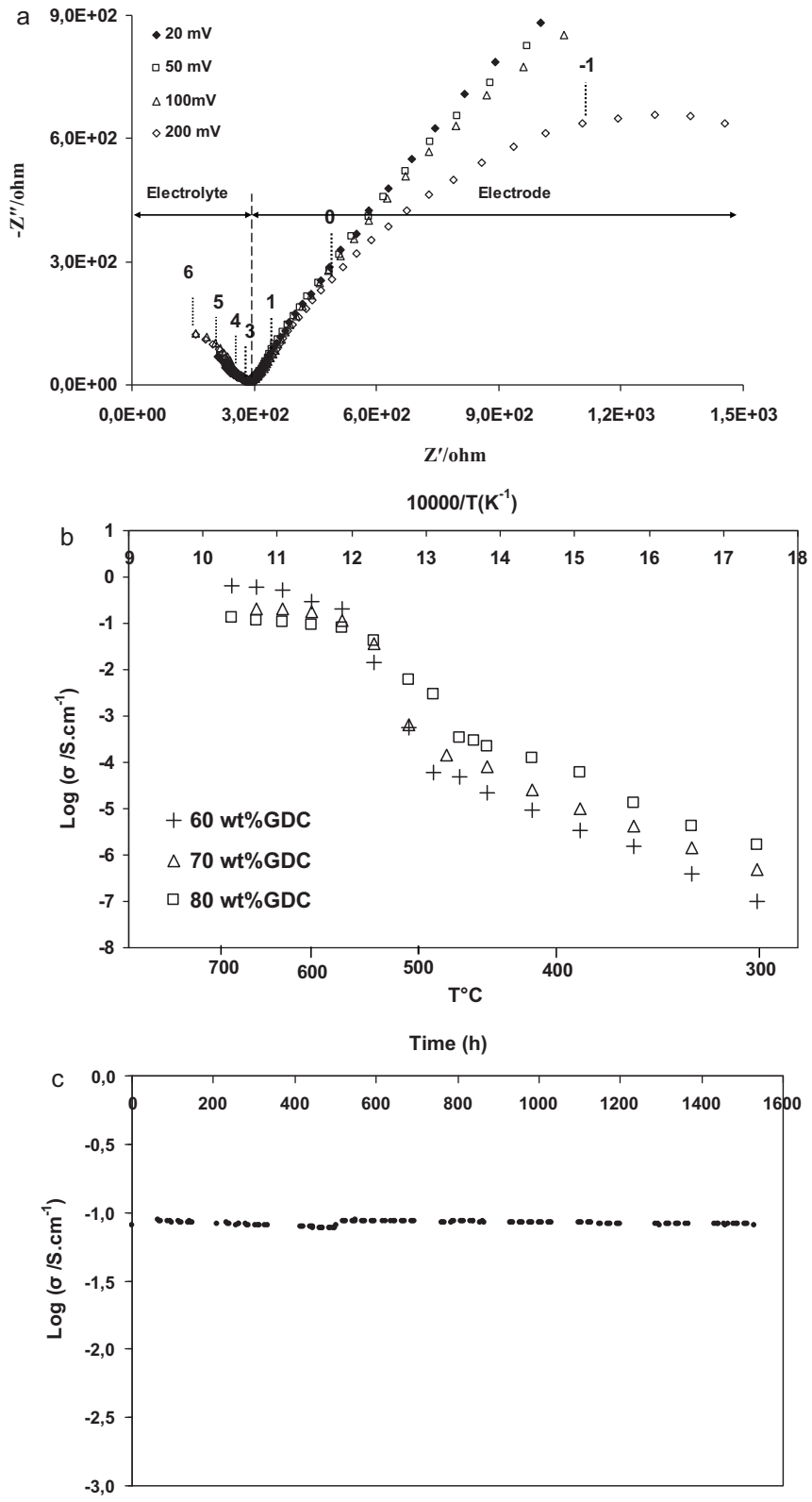

Fig. 12. (a) Nyquist impedance diagrams of GDC/Li_2CO_3–K_2CO_3 (80/20 wt%) composite (annealed at 650 °C for 40 min) at 390 °C under ambient air, with different signal amplitudes from 20 to 200 mV. Frequency logarithms are indicated; (b) Arrhenius plots of the conductivity of GDC/Li_2CO_3–K_2CO_3 under air, annealed at 650 °C for 40 min and sintered at 600 °C for 60 min. Influence of weight ratio GDC/carbonates (in wt%): (+) 60/40, (Δ) 70/30 and (□) 80/20; (c) evolution of the conductivity vs. time for the GDC/Li_2CO_3–K_2CO_3 (70/30 wt%) composite at 600 °C under air.

for 40 min and sintered at 600 °C during 1 h, was measured by impedance spectroscopy as already described [13]. Fig. 12b shows the Arrhenius conductivity diagrams of the three samples. Discontinuities are observed in the log σ vs. $1/T$ plots; in effect, the conductivity increases with the temperature within three different domains: before, during and after the dramatic increase around 485 °C. The change in the slope at this temperature corresponds to the carbonate mixture melting point, which confirms the result

Table 1
Activation energy of GDC/Li_2CO_3–K_2CO_3 composite with different weight ratios at low and high temperature.

Sample GDC–carbonates	Ea (eV) low temperature	Ea (eV) high temperature
80 wt% GDC–20 wt% carbonates	1.21 ± 0.01	0.25 ± 0.05
70 wt% GDC–30 wt% carbonates	1.19 ± 0.01	0.40 ± 0.05
60 wt% GDC–40 wt% carbonates	1.28 ± 0.01	0.60 ± 0.10

obtained with TGA–DTA. Before 485 °C, the ionic conductivity is mainly controlled by oxide ions, after this temperature carbonate ions control the conductivity and around 485 °C, both carbonate and oxides ions are involved. It can also be observed that the sample with the highest amount of carbonates (60/40 wt%) has the lowest conductivity at temperatures lower than the melting point (oxide ions mobility partially disturbed by solid carbonates) and the highest conductivity after the melting point when the ionic conductivity becomes predominantly controlled by molten carbonates. For the two other samples, the situation depends on the carbonate ratio: when it is high it favors the high-temperature conductivity and when it is low it favors the low-temperature conductivity of oxide ions. Table 1 shows the activation energy at low and high temperature (before and after the carbonate melting point). At low temperature, relatively stable values, around 1.2 eV, are obtained. These values, higher than that obtained for pure GDC in our experimental conditions (1 eV) or in the literature (0.8–1 eV), represent most probably the behaviour of oxide ions partially inhibited by the presence of solid carbonates. Other authors found values significantly higher (1.5–2 eV) [38]. At high temperature, the activation energy is not stable and decreases slightly with the increase in the carbonate ratio. Although the accuracy of these values is unlikely to be better than ±0.05–0.1 eV, they are relatively close to the activation energy of pure Li_2CO_3–K_2CO_3 (62:38 mol%), around 0.26 eV [36]. It is not our purpose here to give a deeper insight on the mechanisms involved; they will be detailed in a forthcoming paper fully dedicated to electrical/electrochemical properties.

The conductivity of the sample with the intermediate composition, GDC/Li_2CO_3–K_2CO_3 (70/30 wt%), was measured during 1500 h under air at 600 °C (temperature after the melting point), as described in Fig. 12c. A stable value around 8×10^{-2} S cm^{-1} was obtained, showing as in the TGA/DTA analyses that the carbonate phase remains stable over a relatively long period which is of great interest for the fuel cell application. This value is significantly higher than that of pure GDC, around 1.5×10^{-2} S cm^{-1}.

5. Conclusions

This study was focused mainly on the synthesis of GDC/(Li_2CO_3–K_2CO_3: 72.7–27.3 mol%) composite material, its structural and morphological characterisation, as well as its physical and thermal transformation during thermal cycling. TGA and DTA thermal analyses coupled with mass spectrometry for different compositions and temperatures of the composite processing showed that an endothermic peak detected at high temperature (485 °C) corresponds to the melting point of the Li_2CO_3–K_2CO_3 (62–38 mol%) eutectic. The intensity of this peak increases with the content of carbonates in the composite. The stability of the composite was verified after thermal cycling and an ageing treatment of 168 h, with very low weight losses of both water and CO_2. High-temperature XRD indicated that only GDC peaks are clearly visible. The peaks related to Li_2CO_3 and Li_2CO_3–K_2CO_3, of lower intensity, can also be detected. It can be noted a regular and reversible evolution of the composite with the temperature. With respect to the morphology of the composite, two well-separated phases with different grains and shapes were clearly evidenced. A white and finer phase corresponds to GDC and a gray and coarser phase to carbonates. After sintering, a better densification can be observed, with a microstructure revealing sub-micrometric particles of GDC and a more uniform distribution of the molten carbonate phase. The results obtained with GDC/Li_2CO_3–Na_2CO_3 are quite similar. A preliminary study of the conductivity of GDC/Li_2CO_3–K_2CO_3 (70/30 wt%) showed that a stable value of about 8×10^{-2} S cm^{-1} can be obtained over 1500 h.

Acknowledgements

We wish to acknowledge very warmly Prof. Göran Lindbergh for his valuable scientific advices. XRD facilities in Lille (France) are supported by the Conseil Regional du Nord-Pas de Calais, and the European Regional Development Fund (FEDER).

References

[1] V.V. Kharton, F.M.B. Marques, A. Atkinson, Solid State Ionics 174 (2004) 135.
[2] B. Zhu, M.D. Mat, Int. J. Electrochem. Sci. 1 (2006) 383.
[3] B. Zhu, B.-E. Mellander, in: S.C. Singhal, M. Dokiya (Eds.), Solid Oxide Fuel Cells-VI, The Electrochemical Society, Inc., Pennington, NJ, 1999, p. 244.
[4] B. Zhu, J. Power Sources 93 (2001) 82.
[5] J. Huang, Z. Mao, L. Yang, R. Peng, Electrochem. Solid-State Lett. 8 (2005) A437.
[6] G.Y. Meng, Q.X. Fu, S.W. Zha, C.R. Xia, X.Q. Liu, D.K. Peng, Solid State Ionics 148 (2002) 533.
[7] B. Zhu, X.T. Yang, J. Xu, Z.G. Zhu, S.J. Ji, M.T. Sun, J.C. Sun, J. Power Sources 118 (2003) 47.
[8] B. Zhu, J. Power Sources 114 (2003) 1.
[9] Q.X. Fu, G.Y. Meng, B. Zhu, J. Power Sources 104 (2002) 73.
[10] A. Demin, P. Tsiakaras, E. Gorbova, S. Hramova, J. Power Sources 131 (2004) 231.
[11] T. Schober, Electrochem. Solid-State Lett. 8 (2005) A199.
[12] B. Zhu, I. Albinsson, C. Anderson, K. Borsand, M. Nilsson, B.-E. Mellander, Electrochem. Commun. 8 (2006) 495.
[13] M. Benamira, V. Albin, A. Ringuedé, R.-N. Vannier, A. Bodén, C. Lagergren, M. Cassir, Electrochem. Soc. Trans. 7 (2007) 2261.
[14] M. Benamira, Ph.D. Thesis, University of Paris6, ENSCP (2008).
[15] S. Zha, J. Cheng, Q. Fu, G. Meng, Mater. Chem. Phys. 77 (2002) 594.
[16] S. Li, J. Sn, Int. J. Hydrogen Energy 35 (2010) 2980.
[17] Z. Tang, Q. Lin, B.-E. Mellander, B. Zhu, Int. J. Hydrogen Energy 35 (2010) 2970.
[18] C.M. Lapa, F.M.L. Figueiredo, D.P.F. de Souza, L. Song, B. Zhu, F.M.B. Marques, Int. J. Hydrogen Energy 35 (2010) 2953.
[19] J. Di, M. Chen, C. Wang, J. Zheng, L. Fan, B. Zhu, J. Power Sources 195 (2010) 4695.
[20] R. Raza, X. Wang, Y. Ma, X. Liu, B. Zhu, Int. J. Hydrogen Energy 35 (2010) 2684.
[21] Y. Ma, X. Wang, R. Raza, M. Muhammed, B. Zhu, Int. J. Hydrogen Energy 35 (2009) 2580.
[22] J. Huang, L. Yang, R. Gao, Z. Mao, C. Wang, Electrochem. Commun. 8 (2006) 785.
[23] J. Huang, Z. Mao, Z. Liu, C. Wang, Electrochem. Commun. 9 (2007) 2601.
[24] J. Huang, Z. Mao, Z. Liu, C. Wang, J. Power Sources 175 (2008) 238.
[25] J. Huang, R. Gao, Z. Mao, J. Feng, Int. J. Hydrogen Energy 35 (2010) 2657.
[26] J. Huang, Z. Gao, Z. Mao, Int. J. Hydrogen Energy 35 (2010) 4270.
[27] Y. Li, Z. Rui, C. Xia, M. Anderson, Y.S. Lin, Catal. Today 148 (2009) 303.
[28] C. Xia, Y. Li, Y. Tian, Q. Liu, Y. Zhao, L. Jia, Y. Li, J. Power Sources 188 (2009) 156.
[29] C. Xia, Y. Li, Y. Tian, Q. Liu, Z. Wang, L. Jia, Y. Zhao, Y. Li, J. Power Sources 195 (2010) 3149–3154.
[30] L. Jia, Y. Tian, Q. Liu, C. Xia, J. Yu, Z. Wang, Y. Zhao, Y. Li, J. Power Sources 195 (2010) 5581.
[31] L. Zhang, R. Lan, X. Xu, S. Tao, Y. Jiang, A. Kraft, J. Power Sources 194 (2009) 967.
[32] L. Zhang, R. Lan, C.T.G. Petit, S. Tao, Int. J. Hydrogen Energy 35 (2010) 6934.
[33] W. Liu, Y. Liu, B. Li, T.D. Sparks, X. Wei, W. Pan, Composites Sci Technol. 70 (2010) 181.
[34] M. Sangster, A. D. Pelton, Special Report to the Phase Equilibria Program, American Ceramic Society; Westerville, Ohio, (1987) pp. 4–231.
[35] G.J. Janz, M.R. Lorentz, J. Chem. Eng. Data 6 (1961) 321.
[36] S. Tanase, Y. Miyazaki, M. Yanagida, K. Tanimoto, T. Kodama, Progress Batteries and Solar Cells, vol. 6, 1987.
[37] J.I. Langford, Proc. Int. Conf. on Accuracy of Powder Diffraction II, NIST Special publication, 1992, p. 110, 846.
[38] A. Bodén, J. Di, C. Lagergren, G. Lindbergh, C.H. Wang, J. Power Sources 172 (2007) 520.